

Influence of the stoichiometry on the H-desorption rates measured in solid–gas phase and electrochemical cell for air-exposed LaNi_{5+x} -type alloys

E. Raekelboom^{a,*}, F. Cuevas^a, B. Knosp^b, A. Percheron-Guégan^a

^a Laboratoire de Chimie Métallurgique des Terres Rares CNRS, 2-8 rue Henri Dunant, 94320 Thiais, France

^b SAFT, 111 bd. Alfred Daney, 33074 Bordeaux, France

Received 2 July 2004; received in revised form 21 February 2005; accepted 28 February 2005

Available online 15 July 2005

Abstract

The dehydrogenation of multi-substituted air-exposed LaNi_{5+x} -type materials were investigated both in solid–gas phase and electrochemical cell as a function of their stoichiometry ($x = -0.1, 0.1, 0.3$) while keeping a constant plateau pressure by adjusting their composition. The increase of the stoichiometry is accompanied by an increase of the La/Ce ratio and Ni content. In solid–gas phase, the desorption rates were measured in air-exposed samples upon cycling and were found to be sensitive to the stoichiometry. The oxide formation at the surface produces a significant decrease of the solid–gas phase kinetics. An increase of the overstoichiometry leads to lower rates and capacities as well as restrained decrepitation upon H-cycling. Electrochemical measurements of the high rate dischargeability show constant values within the same range.

© 2005 Elsevier B.V. All rights reserved.

Keywords: Gas–solid reactions; Kinetics; Intermetallics; Hydrogen storage materials, LaNi_5

1. Introduction

Ni-MH batteries are widely used in portable applications such as phones and digital cameras. High power applications (e.g. portable tools) require the electrochemical capacity of the batteries to be delivered in a very short period of time. In order to improve the power delivered by the Ni-MH batteries, the characteristics that influence the desorption rate of the present materials are studied here.

In the AB_{5+x} -type alloys derived from LaNi_5 , the Ni has been partially substituted by manganese and aluminium in order to decrease its equilibrium pressure below 0.1 MPa (for LaNi_5 0.17 MPa at 298 K). High cobalt content (~10 wt.%) was first used since it was found to increase the cycle life by decreasing the decrepitation phenomenon [1,2]. Due to the high cost of cobalt, its content was put down to 5 wt.% in commercialised batteries whereas the overstoichiometry,

having a similar effect on the decrepitation, was increased up to a B/A ratio of 5.3 [3,4]. The mischmetal being a cheaper mixture of rare earths replaces the La.

Electrochemical studies of the kinetic in non-stoichiometric alloys were carried out but have not so far brought conclusive results. In an electrochemical system, the high rate dischargeability which corresponds to the ability of delivering the stored capacity at high discharge current, is a measure of the discharge kinetic. Fukumoto et al. [5] have shown that it increases for alloys of composition $\text{Mm}(\text{Ni}_{3.6}\text{Mn}_{0.4}\text{Al}_{0.3}\text{Co}_{0.7})_z$ when z varies from 0.88 to 1.12 (corresponding to stoichiometry 4.4 to 5.6). On the other hand, Züttel et al. [6] noticed for the same system an optimal composition for $z = 1.02$ (i.e. $\text{AB}_{5.1}$) for which the high rate dischargeability was the best. However, the equilibrium pressure of the plateau P_e is found to increase with it z in the previous experiments. As a result of this, the fast electrochemical discharge kinetics noticed in the previous cases could be due to the increase of the driving forces proportional to $\ln(P_e/P)$.

* Corresponding author. Tel.: +33 1 49 78 12 00; fax: +33 1 49 78 12 03.

Table 1

Composition, stoichiometry (B/A ratio), lattice parameters, cell volume, H-capacities and desorption plateau pressures for $AB_{4.9}$, $AB_{5.1}$ and $AB_{5.3}$ alloys

Composition (targeted/analysed by EPMA)	B/A ratio (targeted/obtained)	Lattice parameters a (Å)/ c (Å)	Cell volume V (Å ³)	H/f.u $T = 45$ °C	P_{des} (MPa) $T = 45$ °C
$La_{0.20}Ce_{0.55}Nd_{0.19}Pr_{0.06}Ni_{3.48}Mn_{0.4}Al_{0.3}Co_{0.72}$ (targeted)	4.9 (targeted)	$a = 4.9762(1)$	86.868(4)	5.05	0.058
$La_{0.21}Ce_{0.55}Nd_{0.20}Pr_{0.05}Ni_{3.44}Mn_{0.38}Al_{0.28}Co_{0.73}$ (analysed by EPMA)	4.87(5) (analysed by EPMA)	$c = 4.0506(1)$			
$La_{0.45}Ce_{0.38}Nd_{0.13}Pr_{0.04}Ni_{3.68}Mn_{0.4}Al_{0.3}Co_{0.72}$ (targeted)	5.1 (targeted)	$a = 4.9874(1)$	87.387(4)	4.84	0.071
$La_{0.44}Ce_{0.38}Nd_{0.14}Pr_{0.03}Ni_{3.71}Mn_{0.40}Al_{0.29}Co_{0.74}$ (analysed by EPMA)	5.15(6) (analysed by EPMA)	$c = 4.0566(1)$			
$La_{0.69}Ce_{0.22}Nd_{0.07}Pr_{0.02}Ni_{3.88}Mn_{0.4}Al_{0.3}Co_{0.72}$ (targeted)	5.3 (targeted)	$a = 5.0039(1)$	88.022(4)	4.08	0.056
$La_{0.69}Ce_{0.22}Nd_{0.077}Pr_{0.013}Ni_{3.93}Mn_{0.41}Al_{0.27}Co_{0.73}$ (analysed by EPMA)	5.33(9) (analysed by EPMA)	$c = 4.0592(1)$			

The aim of the present study is to look at the influence of the stoichiometry on the desorption rates measured in solid–gas phase and electrochemical cell. The alloys were intentionally kept in air to maintain the same starting conditions for the solid–gas phase and electrochemical measurements. Compared to previous results, the influence of the stoichiometry in the AB_{5+x} -type alloys is here investigated independently from the hydride formation and decomposition pressure by increasing the ratio La/Ce with the stoichiometry (see Table 1). The influence that the different compositions of the A and B components may have on the kinetics should therefore not be ignored and will be taken into account when discussing the results.

2. Experimental

2.1. Alloy preparation and characterisation

Alloys of composition $Mm(Ni_{3.58+x}Mn_{0.4}Al_{0.3}Co_{0.72})$ with $x = -0.1, 0.1$ and 0.3 and having high Co content (10 wt.%) were melted in a vacuum induction furnace and annealed for 4 days at 1050 °C. The alloys have been characterised by Rietveld refinement of X-ray diffraction data (XRD) and electron probe microanalysis (EPMA). The alloys were ground in air prior both solid–gas and electrochemical measurements.

2.2. Pressure–composition isotherms and kinetic in solid–gas phase

The Pressure–composition isotherms (PCT) and kinetics have been measured at 45 °C using a Sievert's type device for ~250 mg of ground alloys sieved under 70 µm. The stainless steel sample holder kept in a thermostatic bath, allows a good heat transfert. The variation of the temperature during the reaction does not affect the measurement owing to the slow kinetic and to the relatively small quantity of alloy used. The PCT were established after an activation period of 10 cycles. For the kinetic measurement, a quasi-constant pressure method was used. The absorption curves were obtained at

$P_{abs} = 1$ MPa with a relative variation pressure $\Delta P_{abs}/P_{abs}$ of less than 10%. This variation was higher for desorption ($\Delta P_{des}/P_{des} \sim 40\%$) which was conducted under a pressure of 8×10^{-3} MPa.

2.3. Electrochemical tests

Negative electrodes were prepared from a mixture of the powder alloy with carbon powder for conduction and a cellulosic thickener together with a styrene butadiene rubber binder into a nickel foam, in a weight ratio 97:1:2. The films were cut (2 cm × 2.5 cm) so that it contains 1 g of alloy and pasted on both sides on a nickel grid. The electrodes were cycled electrochemically versus foam positive electrodes of $Ni(OH)_2$ and polyolefin separators soaked in a 8.7N KOH electrolyte in an open polyethylene electrochemical cell. The alloys were preliminary activated during the first cycles. For the high rate dischargeability, capacities were measured using current densities of 1000 down to 50 mA g⁻¹ after a C/10 charge for 16 h.

3. Results and discussion

3.1. Alloy characterisation

All synthesized alloys are found to be single phase having a hexagonal structure (type $CaCu_5$, symmetry $P6/mmm$). Their composition, stoichiometry, lattice parameters volume cell, H-capacities and the absorption plateau pressures are listed in Table 1. The c parameter increases with the stoichiometry due to the replacement of one rare earth atom by a pair of nickel atoms along the c axis [7]. The a parameter was expected to decrease with the stoichiometry but the increase of the La/Ce ratio with the stoichiometry is known to lead to an extension of the a parameter [8].

3.2. Pressure–composition isotherms

Although the cell volumes increase slightly with the stoichiometry, this does not lead to a significant decrease of the

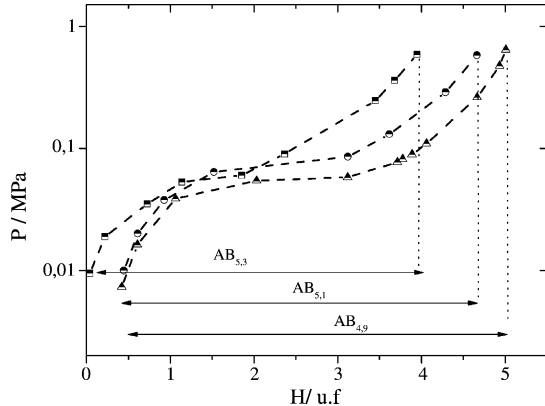


Fig. 1. Pressure–composition isotherms after 10 cycles for the $\text{AB}_{4.9}$, $\text{AB}_{5.1}$ and $\text{AB}_{5.3}$ alloys at 45°C .

desorption plateau pressure (Fig. 1 and Table 1) as it would be expected from the geometric law [9,10]. This is thought to be due to the different valence state of cerium that accounts for the large increase of the cell volumes. The capacity decreases with the overstoichiometry. As already observed by Notten et al. with overstoichiometric $\text{La}(\text{Ni}_{1-z}\text{Cu}_z)_x$ [11] and $\text{La}(\text{Ni}_{1-z}\text{Mn}_z)_x$ ($5 \leq x \leq 6$) [12], this is attributed to the replacement of A type by dumbbells of B type atoms which seems to decrease the hydrogen occupancy of the sites $6m$ and some of the $12o$ [13]. The desorption plateau (not shown for clarity) lies at little lower pressures ($10^{-3} < P_{\text{abs}} - P_{\text{des}} < 4 \times 10^{-3}$ MPa) compared to the absorption isotherms due to a phenomenon of hysteresis.

3.3. Desorption rate measurements

Fig. 2 shows the desorption times for a multielement alloy $\text{AB}_{5.2}$ (Co content of 7.3 wt.%) ground in argon and in air. The slower desorption kinetics measured for the alloys kept in air is thought to be due to the formation of an oxide layer at the surface of the alloys. The composition of the oxide layer at the surface of the present alloys has not been determined here but previous studies have shown they were made of Mm_2O_3 , nickel rich alloy and NiMm_2O_4 [14].

Desorption times for air-exposed samples were measured upon cycling. Fig. 3 shows the time $t_{0.8}$ needed to release 80% of the hydrogen capacities, versus the cycle numbers. The kinetics increase with the cycle number and stabilize after an activation period of five cycles for $\text{AB}_{5.3}$ and $\text{AB}_{5.1}$ and of 10 cycles for $\text{AB}_{4.9}$. After 20 cycles, the times $t_{0.8}$ are found to be eight times higher for $\text{AB}_{5.3}$ than for $\text{AB}_{4.9}$. This is thought to have two possible origins. First the alloy decrepitation upon H-cycling, as seen in the SEM observations (Fig. 4), shows smaller particle size for $\text{AB}_{4.9}$ alloy compared to $\text{AB}_{5.3}$. The oxide-free surfaces created during the decrepitation allow more rapid H-kinetic for low-stoichiometric alloys. Secondly, the increase of the La/Ce ratio and the nickel for $\text{AB}_{5.3}$ content may lead to a denser oxide layer acting as a barrier for the hydrogen desorption.

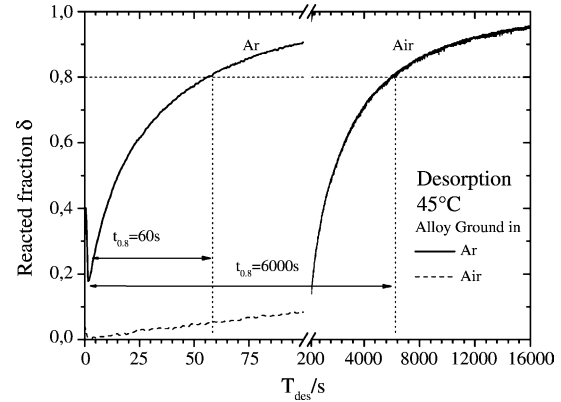


Fig. 2. Plot of the reacted fraction δ vs. time t_{des} for an alloy $\text{AB}_{5.2}$ ($\text{La}_{0.62}\text{Ce}_{0.25}\text{Nd}_{0.11}\text{Pr}_{0.02}\text{Ni}_{3.99}\text{Mn}_{0.40}\text{Al}_{0.28}\text{Co}_{0.55}$) ground in air and argon.

The curves of the reacted fraction against time are shown at Fig. 5 for the three alloys during the tenth desorption. The solid–gas desorption rates $R = d\delta/dt$ at $\delta = 0.5$ for the tenth desorption are shown in Fig. 6 together with the maximum discharge rate R_m obtained from the electrochemical measurements. The discharge rate R_m is the reciprocal of the slope of the linear regression of the discharge capacity as a function of the discharge current. In an electrochemical system, the high rate dischargeability is a measure of the discharge kinetic. The rate R_m are found to be independent of the composition of the alloys (Fig. 6). This may be explained by the fact that the initial oxide layers are removed during the cycling in contact with the electrolyte. The penetration of the hydrogen through the corrosion layer now limits the kinetics. A corrosion layer made of $\text{Mm}(\text{OH})_3$ as well as nanoparticules of Ni and Co are known to form in contact with the electrolyte during the cycling [14,15]. The constant values of R_m as the stoichiometry increases seem to indicate that the corrosion layer covers continuously the new surface originated from the decrepitation and that the composition of the corrosion layer is similar within the non-stoichiometric alloys.

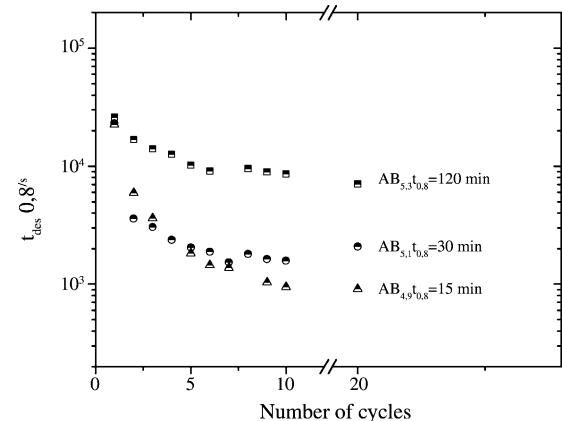
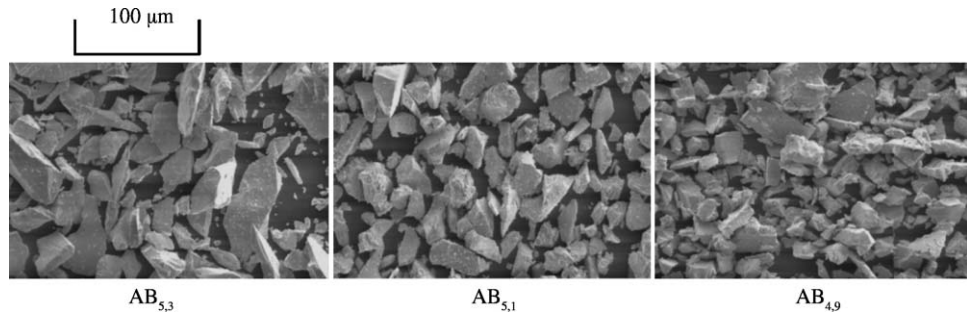
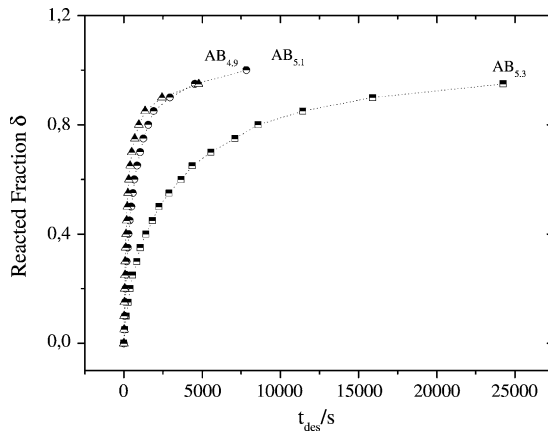
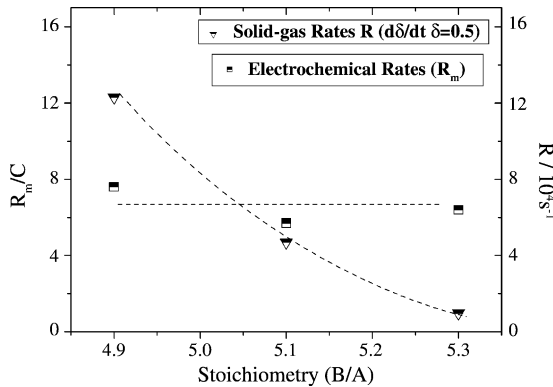


Fig. 3. Plot of the time $t_{0.8}$ needed to release 80% of the hydrogen capacities, versus the cycle numbers for the $\text{AB}_{4.9}$, $\text{AB}_{5.1}$ and $\text{AB}_{5.3}$ alloys at 45°C .

Fig. 4. SEM images of the alloys $AB_{5.3}$, $AB_{5.1}$ and $AB_{4.9}$ after cycling.Fig. 5. Plot of reacted fraction δ vs. time t_{des} for the $AB_{4.9}$, $AB_{5.1}$ and $AB_{5.3}$ alloys at $45^\circ C$.Fig. 6. Evolution of the maximum discharge rate R_m and the solid–gas desorption rate $R = d\delta/dt$ (at $\delta = 0.5$) with the stoichiometry for the alloys $AB_{4.9}$, $AB_{5.1}$ and $AB_{5.3}$ at $45^\circ C$. (a nC rate corresponds to the discharge of the capacity in $1/n$ hour).

4. Conclusion

Dehydrogenation kinetics have been studied in air-exposed $LaNi_{5+x}$ -type alloys while varying the stoichiometry independently from the hydride formation/decomposition pressure. In order to achieve a constant pressure, the increase of the stoichiometry is accompanied by an increase of the La/Ce ratio and Ni content. The oxide formation at the surface of the alloys is thought to lead to slower kinetics compared

with alloys kept in Ar. When the stoichiometry of the alloys is increased, the slower solid–gas kinetics take their origin in the reduced decrepitation and in the modification of the composition of the oxide layer made of Mm_2O_3 at the surface acting as a barrier for the hydrogen. The electrochemical high rate dischargeability is found to be constant with the stoichiometry due to the continuous corrosion that affects the new surface generated from the decrepitation during the cycling.

Acknowledgements

Authors would like to thank the French Ministry of Research for the financial support, J.-L. Pastol and E. Leroy for the SEM and EPMA analysis.

References

- [1] T. Sakai, K. Oguro, H. Miyamura, N. Kuriyama, A. Kato, H. Ishikawa, C. Iwakura, J. Less-Common Met. 161 (1990) 193.
- [2] G.D. Adzic, J.R. Johnson, S. Mukerjee, J.M. Breen, J.J. Reilly, J. Alloys Compd. 253/254 (1997) 579.
- [3] P.H.L. Notten, J.L.C. Daams, R.E.F. Einerhand, J. Alloys Comp. 210 (1994) 233.
- [4] M. Latroche, P.H.L. Notten, A. Percheron-Guégan, J. Alloys Compd. 253/254 (1997) 295.
- [5] Y. Fukumoto, M. Miyamoto, H. Inoue, M. Matsuoka, C. Iwakura, J. Alloys Compd. 231 (1995) 562.
- [6] A. Züttel, V. Güther, A. Otto, M. Bärtsch, R. Kötz, D. Chartouni, Ch. Nützenadel, L. Schlapbach, J. Alloys Compd. 293–295 (1999) 663.
- [7] K.H.J. Buschow, H.H. Van Mal, J. Less-Common Met. 29 (1972) 203.
- [8] J.-M. Joubert, M. Latroche, A. Percheron-Guégan, F. Bourée-Vigneron, J. Alloys Compd. 275–277 (1998) 118.
- [9] J.-C. Achart, A. Percheron-Guégan, H. Fiaz, F. Briaucourt, F. Demany, in: Proceedings of the 2nd International Congress on Hydrogen in Metals, Paris, (1977) 1E12.
- [10] M.H. Mendelsohn, D.M. Gruen, A.E. Dwight, Nature 269 (1977) 45.
- [11] P.H.L. Notten, R.E.F. Einerhand, J.L.C. Daams, J. Alloys Compd. 210 (1994) 233.
- [12] P.H.L. Notten, M. Latroche, A. Percheron-Guégan, J. Electrochem. Soc. 146 (1999) 3181.
- [13] M. Latroche, J.-M. Joubert, A. Percheron-Guégan, F. Bourée-Vigneron, J. Solid State Chem. 177 (2004) 1219.
- [14] F. Maurel, B. Knosp, M. Backhaus-Ricoult, J. Electrochem. Soc. 147 1 (2000) 78.
- [15] J.J.G. Willems, Suppl. Phillips J. Res. 39 Suppl. 1 (1984) 1.